Available online at www.sciencedirect.com
ScienceDirect
Journal of Computational Physics 227 (2008) 5090–5104
JOURNAL OF COMPUTATIONAL PHYSICS
www.elsevier.com/locate/jcp

Dispersive properties of multisymplectic integrators

C.M. Schober *, T.H. Wlodarczyk

Department of Mathematics, University of Central Florida, P.O. Box 161364, Orlando 32816-1364, United States

Received 24 September 2007; received in revised form 16 January 2008; accepted 17 January 2008
Available online 1 February 2008

Abstract

Multisymplectic (MS) integrators, i.e. numerical schemes which exactly preserve a discrete space–time symplectic structure, are a new class of structure preserving algorithms for solving Hamiltonian PDEs. In this paper we examine the dispersive properties of MS integrators for the linear wave and sine-Gordon equations. In particular a leapfrog in space and time scheme (a member of the Lobatto Runge–Kutta family of methods) and the Preissman box scheme are considered. We find the numerical dispersion relations are monotonic and that the sign of the group velocity is preserved. The group velocity dispersion (GVD) is found to provide significant information and succinctly explain the qualitative differences in the numerical solutions obtained with the different schemes. Further, the numerical dispersion relations for the linearized sine-Gordon equation provides information on the ability of the MS integrators to capture the sine-Gordon dynamics. We are able to link the numerical dispersion relations to the total energy of the various methods, thus providing information on the coarse grid behavior of MS integrators in the nonlinear regime.

Keywords: Multisymplectic methods; Box schemes; Leapfrog method; Dispersion relation; Sine-Gordon equation; Double-pole soliton

1. Introduction

Symplectic integrators have proven to be robust, efficient and very accurate in preserving the long-time behavior of solutions of Hamiltonian ODEs [11]. These results made it natural to consider extending symplecticity to Hamiltonian PDEs and to develop the concept of a space–time multisymplectic structure [15,4,6]. In [15] Marsden and Shkoller developed the multisymplectic structure of Hamiltonian PDEs from a Lagrangian formulation using a variational principle. In this paper we adopt the approach of Bridges and Reich and consider Hamiltonian PDEs of the form [6]

$$\boldsymbol{L}\mathbf{z}_t + \boldsymbol{K}\mathbf{z}_x = \nabla_{\mathbf{z}} S, \quad \mathbf{z} \in \mathbb{R}^d, \tag{1}$$

where $\boldsymbol{L}$ and $\boldsymbol{K}$ are $d \times d$, skew-symmetric matrices, and $S : \mathbb{R}^d \to \mathbb{R}$ is a smooth function of the state variable $\mathbf{z}$. System (1) is multisymplectic (MS) in the sense that associated with $\boldsymbol{L}$ and $\boldsymbol{K}$ are the two-forms,

* Corresponding author.
E-mail address: cschober@mail.ucf.edu (C.M. Schober).

0021-9991/$ - see front matter © 2008 Elsevier Inc. All rights reserved.
doi:10.1016/j.jcp.2008.01.026

$$\omega = \frac{1}{2}(\mathrm{d}\mathbf{z} \wedge \boldsymbol{L}\,\mathrm{d}\mathbf{z}), \quad \kappa = \frac{1}{2}(\mathrm{d}\mathbf{z} \wedge \boldsymbol{K}\,\mathrm{d}\mathbf{z}), \tag{2}$$

which define a space–time multisymplectic structure governed by the multisymplectic conservation law (MSCL)

$$\partial_t \omega + \partial_x \kappa = 0. \tag{3}$$

Eq. (3), which is a local property, is derived directly from (1) and generalizes the symplectic conservation law of Hamiltonian ODEs. The multisymplectic structure naturally gives rise to local conservation laws typically associated with Nöthers theorem [15]. In fact, in the presence of a MS structure, the invariance of the Hamiltonian $S(z)$ with respect to space–time shifts implies the local energy and momentum conservation laws,

$$\text{LECL}: \quad \partial_t E + \partial_x F = 0, \quad E = S(\mathbf{z}) + \frac{1}{2}\mathbf{z}_x^T \boldsymbol{K}\mathbf{z}, \quad F = -\frac{1}{2}\mathbf{z}_t^T \boldsymbol{K}\mathbf{z}, \tag{4}$$

$$\text{LMCL}: \quad \partial_t I + \partial_x G = 0, \quad G = S(\mathbf{z}) + \frac{1}{2}\mathbf{z}_t^T \boldsymbol{L}\mathbf{z}, \quad I = -\frac{1}{2}\mathbf{z}_x^T \boldsymbol{L}\mathbf{z}, \tag{5}$$

respectively.

Multisymplectic integrators are defined to be discretizations of (1) for which a discrete form of the MSCL (3) holds. A thorough analysis of multisymplectic integrators is far from complete as even this definition is in the process of being refined. For example, partitioned Runge–Kutta methods applied to (1) formally satisfy discrete multisymplectic conservation laws, yet do not always produce well defined numerical schemes [8]. Additional constraints such as requiring the scheme to be compact or to be a one step method in space and time have been proposed [20,10]. An open question is which properties, such as compactness or conservation of wave action or preservation of the dispersion relation, are important for a multisymplectic method to inherit under discretization [9]. Nonetheless, excellent long-time preservation of the local energy and momentum conservations laws has been established in numerical studies of multisymplectic integrators for the nonlinear Schrödinger equation [19,12]. The improved preservation of the local conservation laws is also reflected in an improved preservation of complicated phase space structures [14].

In the study of wave motion the dispersion relation and group velocity are fundamental concepts. A wave packet is a superposition of modes with different wavenumbers. Errors in the phase and group velocities lead to modes traveling with an incorrect speed which can destroy the qualitative features of the solution [21]. Recent results on symplectic and multisymplectic schemes for the Korteweg de Vries equation show that the MS Preissman box scheme, a member of the Gauss–Legendre Runge–Kutta (GLRK) family, qualitatively preserve the dispersion relation of any hyperbolic system [2]. This result was extended for linear PDEs to cover general s-stage GLRK methods [10]. It was found that the discrete dispersion relation for GLRK methods is monotonic and the group velocity is of constant sign.

From the perspective of integrable nonlinear PDEs, e.g. the sine-Gordon or the Korteweg de Vries equations, the dispersion relation of the associated linearized equation is especially significant. Initial-value problems for integrable nonlinear PDEs can be solved by the inverse scattering transform (IST) [1]. The first step is to calculate the scattering data of the waveform $u(x, t_0)$ via the direct scattering transform. The scattering data is then evolved to any time t^* according to equations that depend on the dispersion relation of the associated linearized equation. The solution is then recovered by the inverse scattering transform.

In this paper we further examine the dispersive properties of MS integrators for the linear wave and sine-Gordon equations. Specifically a leapfrog in space and time scheme (MSLF), a member of the Lobatto Runge–Kutta family of methods, and the Preissman box (MSBS) scheme are examined, as well as, for comparative purposes, a standard explicit Runge–Kutta scheme. For the multisymplectic schemes we show the numerical dispersion relations are monotonic, the sign of the group velocity is preserved, and obtain a relationship between the group velocities of the different numerical schemes. Further, we find the group velocity dispersion (GVD) provides significant information and succinctly explains the differences in the numerical solutions obtained with the different schemes, e.g. why some schemes "shed" oscillatory waves off the front of the pulse and others off the back.

Finally, we examine whether the numerical dispersion relations for the linearized sine-Gordon (sG) equation provide information on the ability of the MS integrators to capture the nonlinear sine-Gordon dynamics. For the kink–antikink solutions of the sine-Gordon equation we observe shedding of oscillatory waves which, as for

the linear wave equation, can be explained through the errors in the group velocity. A more striking example of the impact of errors in the dispersion relation is provided by the double-pole soliton solution of the sine-Gordon equation. We observe distinctly different convergence patterns for the MSBS and MSLF schemes. The MSBS solutions exhibit breather-like behavior, while the MSLF solutions exhibit kink–antikink behavior. From the dispersion analysis we are able to link the numerical dispersion relations to the total energy of the various methods, thus providing information on the coarse grid behavior of MS integrators in the nonlinear regime.

2. Multisymplectic PDEs

2.1. The wave and sine-Gordon equations

An example of a MS PDE is provided by the equation

$$u_{tt} - u_{xx} + \chi \sin u = 0, \tag{6}$$

where χ allows us to study both the wave ($\chi = 0$) and sine-Gordon ($\chi = 1$) equations. By introducing new variables, $v = u_t$ and $w = -u_x$, Eq. (6) can be written in MS form where

$$\boldsymbol{L} = \begin{bmatrix} 0 & 1 & 0 \\ -1 & 0 & 0 \\ 0 & 0 & 0 \end{bmatrix}, \quad \boldsymbol{K} = \begin{bmatrix} 0 & 0 & 1 \\ 0 & 0 & 0 \\ -1 & 0 & 0 \end{bmatrix}, \quad \mathbf{z} = \begin{bmatrix} u \\ v \\ w \end{bmatrix}, \quad S = \frac{1}{2}(w^2 - v^2) + \chi \cos u. \tag{7}$$

By observing that v and w satisfy the extra constraint $w_t + v_x = -u_{xt} + u_{tx} = 0$ and introducing a Lagrange multiplier p satisfying $p_x = -v + u_t$ and $p_t = w + u_x$, an improved MS form can be obtained where

$$\boldsymbol{L} = \begin{bmatrix} 0 & 1 & 0 & 0 \\ -1 & 0 & 0 & 0 \\ 0 & 0 & 0 & 1 \\ 0 & 0 & -1 & 0 \end{bmatrix}, \quad \boldsymbol{K} = \begin{bmatrix} 0 & 0 & 1 & 0 \\ 0 & 0 & 0 & 1 \\ -1 & 0 & 0 & 0 \\ 0 & -1 & 0 & 0 \end{bmatrix}, \quad \mathbf{z} = \begin{bmatrix} u \\ v \\ w \\ p \end{bmatrix} \tag{8}$$

and $S(\mathbf{z})$ is the same as before [5,14]. This example shows that the MS structure of a PDE is not unique.

Both MS formulations have local energy and momentum conservation laws given by [6,14]

$$\partial_t E + \partial_x F = 0, \quad \text{where } E = \frac{1}{2}(v^2 + w^2) - \chi \cos u, \quad F = vw \tag{9}$$

and

$$\partial_t I + \partial_x G = 0, \quad \text{where } I = vw, \quad G = \frac{1}{2}(v^2 + w^2) + \chi \cos u. \tag{10}$$

The existence of integrals of motion and local conservation laws is an important feature of a system. If periodic boundary conditions are considered, the global energy and momentum are given by

$$\mathcal{E} = \int_0^L E \, \mathrm{d}x = \int_0^L \frac{1}{2}(v^2 + w^2) - \cos u \, \mathrm{d}x, \quad \mathcal{I} = \int_0^L I \, \mathrm{d}x = \int_0^L vw \, \mathrm{d}x.$$

3. Multisymplectic discretizations

In this section we construct MS discretizations by concatenating symplectic discretizations in space and time.

3.1. MS leapfrog scheme

We begin by introducing the following finite difference operators

$$D_x \mathbf{z}_j^n = \frac{\mathbf{z}_{j+1}^n - \mathbf{z}_j^n}{\Delta x}, \quad D_t \mathbf{z}_j^n = \frac{\mathbf{z}_j^{n+1} - \mathbf{z}_j^n}{\Delta t} \tag{11}$$

and averaging operators

$$M_x \mathbf{z}_j^n = \frac{1}{2}(\mathbf{z}_{j+1}^n + \mathbf{z}_j^n), \quad M_t \mathbf{z}_j^n = \frac{1}{2}(\mathbf{z}_j^{n+1} + \mathbf{z}_j^n). \tag{12}$$

Applying symplectic Euler discretizations, in both space and time, to Eq. (1) gives the following discretization

$$\boldsymbol{L}^+ D_t \mathbf{z}_j^n + \boldsymbol{L}^- D_t \mathbf{z}_j^{n-1} + \boldsymbol{K}^+ D_x \mathbf{z}_j^n + \boldsymbol{K}^- D_x \mathbf{z}_{j-1}^n = \nabla_{\mathbf{z}} S(\mathbf{z}_j^n), \tag{13}$$

where $\boldsymbol{L}^\pm$ and $\boldsymbol{K}^\pm$ are defined such that

$$\boldsymbol{L} = \boldsymbol{L}^+ + \boldsymbol{L}^-, \quad \boldsymbol{L}^- = -(\boldsymbol{L}^+)^T, \quad \boldsymbol{K} = \boldsymbol{K}^+ + \boldsymbol{K}^-, \quad \boldsymbol{K}^- = -(\boldsymbol{K}^+)^T.$$

Proposition 1. *Scheme (13) is a MS discretization.*

Proof. Here we present a more detailed version of the proof given by Moore and Reich [16]. To show that (13) is a MS discretization we take the wedge product between the variational equation and $\mathbf{dz}_j^n$

$$\mathbf{dz}_j^n \wedge (\boldsymbol{L}^+ D_t \mathbf{dz}_j^n + \boldsymbol{L}^- D_t \mathbf{dz}_j^{n-1} + \boldsymbol{K}^+ D_x \mathbf{dz}_j^n + \boldsymbol{K}^- D_x \mathbf{dz}_{j-1}^n) = \mathbf{dz}_j^n \wedge S_{\mathbf{zz}} \mathbf{dz}_j^n. \tag{14}$$

Since $S_{\mathbf{zz}}$ is symmetric, the right hand side vanishes. The time-derivative part of (14) becomes

$$\begin{aligned}
\mathbf{dz}_j^n \wedge (\boldsymbol{L}^+ D_t \mathbf{dz}_j^n + \boldsymbol{L}^- D_t \mathbf{dz}_j^{n-1}) &= \mathbf{dz}_j^n \wedge \boldsymbol{L}^+ D_t \mathbf{dz}_j^n + D_t \mathbf{dz}_j^{n-1} \wedge \boldsymbol{L}^+ \mathbf{dz}_j^n \\
&= \mathbf{dz}_j^n \wedge \boldsymbol{L}^+ \left(\frac{\mathbf{dz}_j^{n+1} - \mathbf{dz}_j^n}{\Delta t} \right) + \left(\frac{\mathbf{dz}_j^n - \mathbf{dz}_j^{n-1}}{\Delta t} \right) \wedge \boldsymbol{L}^+ \mathbf{dz}_j^n \\
&= \frac{1}{\Delta t}(\mathbf{dz}_j^n \wedge \boldsymbol{L}^+ \mathbf{dz}_j^{n+1} - \mathbf{dz}_j^{n-1} \wedge \boldsymbol{L}^+ \mathbf{dz}_j^n) = D_t(\mathbf{dz}_j^{n-1} \wedge \boldsymbol{L}^+ \mathbf{dz}_j^n) \\
&= D_t(\mathbf{dz}_j^n \wedge \boldsymbol{L}^- \mathbf{dz}_j^{n-1}) = \frac{1}{2} D_t(\mathbf{dz}_j^{n-1} \wedge \boldsymbol{L}^+ \mathbf{dz}_j^n + \mathbf{dz}_j^n \wedge \boldsymbol{L}^- \mathbf{dz}_j^{n-1}).
\end{aligned}$$

Similarly, the space-derivative part of (14) becomes

$$\mathbf{dz}_j^n \wedge \boldsymbol{K}^+ D_x \mathbf{dz}_j^n + \mathbf{dz}_j^n \wedge \boldsymbol{K}^- D_x \mathbf{dz}_{j-1}^n = \frac{1}{2} D_x(\mathbf{dz}_{j-1}^n \wedge \boldsymbol{K}^+ \mathbf{dz}_j^n + \mathbf{dz}_j^n \wedge \boldsymbol{K}^- \mathbf{dz}_{j-1}^n).$$

From this we obtain the discrete MS conservation law

$$D_t \omega_j^n + D_x \kappa_j^n = 0, \tag{15}$$

where

$$\omega_j^n = \frac{1}{2}(\mathbf{dz}_j^{n-1} \wedge \boldsymbol{L}^+ \mathbf{dz}_j^n + \mathbf{dz}_j^n \wedge \boldsymbol{L}^- \mathbf{dz}_j^{n-1}), \tag{16a}$$

$$\kappa_j^n = \frac{1}{2}(\mathbf{dz}_{j-1}^n \wedge \boldsymbol{K}^+ \mathbf{dz}_j^n + \mathbf{dz}_j^n \wedge \boldsymbol{K}^- \mathbf{dz}_{j-1}^n). \qquad \square \tag{16b}$$

Notice that (15) is a symplectic Euler discretization, in both space and time, of the MSCL (3), proving that (13) is indeed a MS discretization. For PDEs involving only second derivatives this scheme provides symplectic leapfrog discretizations in space and time. We refer to (13) as the MS leapfrog (MSLF) scheme when applied to the sine-Gordon and linear wave equations.

3.2. MS Preissman box scheme

Using symplectic implicit midpoint discretizations in space and in time yields the following box scheme,

$$\boldsymbol{L} D_t M_x \mathbf{z}_j^n + \boldsymbol{K} D_x M_t \mathbf{z}_j^n = \nabla_{\mathbf{z}} S(M_t M_x \mathbf{z}_j^n), \tag{17}$$

which has been shown to be a MS discretization [6,19] and which we denote as MSBS.

3.3. MS Discretizations for the wave and sine-Gordon equations

3.3.1. MSLF for the wave and sine-Gordon equations

To obtain the leapfrog MS discretization (13) of the sine-Gordon Eq. (7) we use the matrices

$$\boldsymbol{L}^+ = \begin{bmatrix} 0 & 1 & 0 \\ 0 & 0 & 0 \\ 0 & 0 & 0 \end{bmatrix}, \quad \boldsymbol{K}^+ = \begin{bmatrix} 0 & 0 & 1 \\ 0 & 0 & 0 \\ 0 & 0 & 0 \end{bmatrix}, \tag{18}$$

which in system form becomes

$$D_t v_j^n + D_x w_j^n = -\chi \sin(u_j^n), \tag{19a}$$
$$D_t u_j^{n-1} = v_j^n, \tag{19b}$$
$$D_x u_{j-1}^n = -w_j^n. \tag{19c}$$

System (19) can be reduced to the single equation

$$D_t^2 u_j^{n-1} - D_x^2 u_{j-1}^n + \chi \sin u_j^n = 0. \tag{20}$$

3.3.2. MSBS for the wave and sine-Gordon equations

Applying box scheme (17) to the sine-Gordon Eq. (8) results in the system

$$D_t M_x v_j^n + D_x M_t w_j^n = -\chi \sin(M_t M_x u_j^n), \tag{21a}$$
$$D_t M_x u_j^n - D_x M_t p_j^n = M_t M_x v_j^n, \tag{21b}$$
$$D_t M_x p_j^n - D_x M_t u_j^n = M_t M_x w_j^n, \tag{21c}$$
$$D_t M_x w_j^n + D_x M_t v_j^n = 0, \tag{21d}$$

which can also be reduced to the single equation

$$D_t^3 M_x^2 u_j^n - D_t D_x^2 M_t^2 u_j^n + \chi D_t M_t M_x \sin(M_t M_x u_j^n) = 0. \tag{22}$$

3.3.3. Non-symplectic explicit Runge–Kutta scheme

For comparison purposes we consider the discretization obtained by using the symplectic Euler in space together with a standard second order explicit Runge–Kutta method in time, and denote this scheme as ERK.

4. Dispersion relations

The general solution to a linear PDE can be expressed as

$$u(x,t) = \int_{-\infty}^{\infty} A(k) \mathrm{e}^{\mathrm{i}(kx - \omega(k)t)} \, \mathrm{d}k, \tag{23}$$

where $\omega(k)$ can be found by assuming each mode (or "wave") $A\mathrm{e}^{\mathrm{i}(kx-\omega t)}$ is itself a solution of the linear PDE, resulting in a dispersion relation

$$D(\omega, k) = 0.$$

For example, the sine-Gordon equation linearized about $u = 0$,

$$u_{tt} - u_{xx} + \chi u = 0 \tag{24}$$

has a dispersion relation given by

$$D(\omega, k) = \omega^2 - k^2 - \chi = 0. \tag{25}$$

Each wave travels with a phase velocity $v_p(k) = \omega/k$. In a non-dispersive system, such as the wave equation ($\chi = 0$), every wave has the same phase velocity ($v_p = c_0$) and the solution for $t > 0$ is just the initial condition translated through space:

$$u(x,t) = \int_{-\infty}^{\infty} A(k) e^{ik(x-c_0 t)} dk = u(x - c_0 t, 0).$$

In dispersive systems, the important propagation velocity is the group velocity, $V_g(k) = w'(k)$, which is usually a function of the wavenumber k. In this case $w''(k) \neq 0$ and waves with different wavenumbers travel with different phase velocities. This results in group velocity dispersion (GVD), which is proportional to $w''(k)$, and ultimately causes spatial spreading of the wave packet. Using asymptotic analysis one can show that for slowly varying systems, and for sufficiently long times, each wavenumber k dominates the solution in a region defined by $x \approx w'(k)t$ with the dominant contribution given by

$$A(k)\sqrt{\frac{2\pi}{t|w''(k)|}} \exp\left\{ i\left(kx - w(k)t - \frac{\pi}{4} \operatorname{sgn} w''(k) \right) \right\}.$$

Because of their significance, we use the group velocity and the GVD as diagnostics for interpreting the numerical results.

4.1. Numerical dispersion relations

The dispersive properties of the discretizations can be studied by calculating their numerical dispersion relations. To do so, we start with the discretizations of the linearized sine-Gordon/ wave Eq. (24) associated with the MSBS, MSLF, and ERK schemes in their single equation format:

$$\text{MSBS}: \quad D_t^3 M_x^2 u_j^n - D_t D_x^2 M_t^2 u_j^n + \chi D_t M_t^2 M_x^2 u_j^n = 0, \tag{26a}$$

$$\text{MSLF}: \quad D_t^2 u_j^{n-1} - D_x^2 u_{j-1}^n + \chi u_j^n = 0, \tag{26b}$$

$$\text{ERK}: \quad D_t^2 u_j^{n-1} - D_x^2 u_{j-1}^n + \chi u_j^n = -\frac{1}{4}\Delta t^2 D_x^4 u_{j-2}^{n-1} \tag{26c}$$

and assume a discrete general solution of the form

$$\sum_{\bar{k}} A e^{i(\bar{k}\, j - \bar{\omega}\, n)}, \quad \bar{k} = k\Delta x, \quad \bar{\omega} = \omega \Delta t, \tag{27}$$

where as before, each mode is a solution provided $\bar{k}$ and $\bar{\omega}$ satisfy a numerical dispersion relation

$$D_N(\bar{\omega}, \bar{k}) = 0.$$

For Eqs. (26), the corresponding numerical dispersion relations are given by

$$\text{MSBS}: \quad \left(\frac{2}{\Delta t}\tan\frac{\bar{\omega}}{2}\right)^2 - \left(\frac{2}{\Delta x}\tan\frac{\bar{k}}{2}\right)^2 - \chi = 0, \tag{28a}$$

$$\text{MSLF}: \quad \left(\frac{2}{\Delta t}\sin\frac{\bar{\omega}}{2}\right)^2 - \left(\frac{2}{\Delta x}\sin\frac{\bar{k}}{2}\right)^2 - \chi = 0, \tag{28b}$$

$$\text{ERK}: \quad \left(\frac{2}{\Delta t}\sin\frac{\bar{\omega}}{2}\right)^2 - \left(\frac{2}{\Delta x}\sin\frac{\bar{k}}{2}\right)^2 - \chi = \frac{\Delta t^2}{4}\left[\left(\frac{2}{\Delta x}\sin\frac{\bar{k}}{2}\right)^2 + \chi\right]^2, \tag{29}$$

where (29) is to leading order. The MSBS and MSLF schemes preserve the form of the analytical dispersion relation. Generalizing [3,10] we find the exact relationship is given by the following proposition:

Proposition 2. *The MS schemes (28) qualitatively preserve the dispersion relation of the linear PDE. Specifically, there exist diffeomorphisms ψ_1 and ψ_2 satisfying the exact dispersion relationship*

$$D_N(\bar{\omega}, \bar{k}) = D(\psi_1(\bar{\omega}), \psi_2(\bar{k})) = \psi_1^2 - \psi_2^2 - \chi = 0, \tag{30}$$

where

$$MSBS: \quad (\psi_1(\bar{\omega}), \psi_2(\bar{k})) = \left(\frac{2}{\Delta t}\tan\frac{\bar{\omega}}{2}, \frac{2}{\Delta x}\tan\frac{\bar{k}}{2}\right), \tag{31a}$$

$$MSLF: \quad (\psi_1(\bar{\omega}), \psi_2(\bar{k})) = \left(\frac{2}{\Delta t}\sin\frac{\bar{\omega}}{2}, \frac{2}{\Delta x}\sin\frac{\bar{k}}{2}\right) \tag{31b}$$

for $-\pi < \bar{k} < \pi$, *and* $-\pi < \bar{\omega} < \pi$.

Diffeomorphisms can also be found for other MS integrators such as the MS box scheme applied to (7) rather than (8), and the MS scheme obtained by applying an implicit midpoint step in time and a leapfrog discretization in space [18].

4.2. The linear wave equation

The significance of Proposition 2 for the non-dispersive wave equation (Eq. (24) with $\chi = 0$) can be seen in Figs. 1–3 which show the dispersion curves $\bar{\omega}(\bar{k})$, the group velocity $\bar{\omega}'(\bar{k})$, and the group velocity dispersion $\bar{\omega}''(\bar{k})$ for the exact (25) and numerical (28a), (28b), (29) dispersion relations for three different values of the mesh ratio $\lambda = \Delta t/\Delta x$, i.e. $\lambda = 0.1, 0.4, 0.7$. The exact relation is given by $\bar{\omega} = \lambda\bar{k}$. Each plot is shown only for $0 \leqslant \bar{k} \leqslant \pi$ and $0 \leqslant \bar{\omega} \leqslant \pi$ since the dispersion relations are symmetric with respect to the origin.

Several observations can be made. The first is that the existence of diffeomorphisms (31) is not enough to preserve the qualitative features of the analytical solution. Since the exact dispersion relation is linear and the numerical dispersion relations are nonlinear, all of the schemes introduce numerical dispersion. Secondly, the

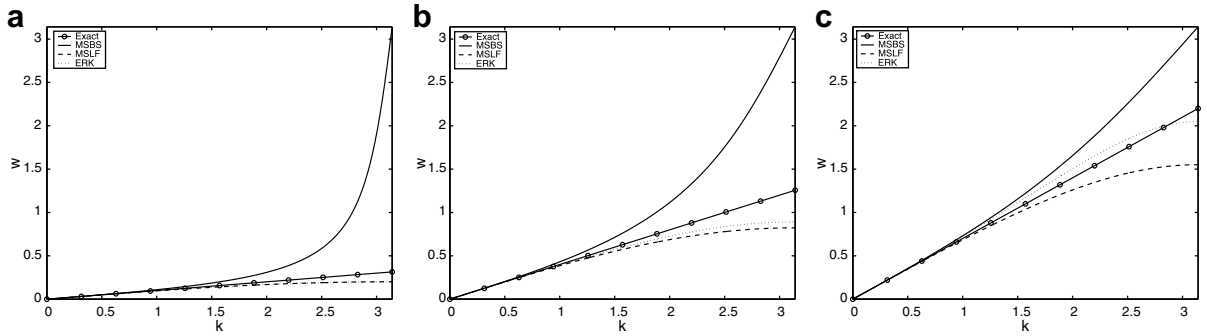

Fig. 1. Dispersion relations for the MSBS, MSLF and ERK discretizations of linear wave equation for (a) $\lambda = 0.1$, (b) $\lambda = 0.4$ and (c) $\lambda = 0.7$.

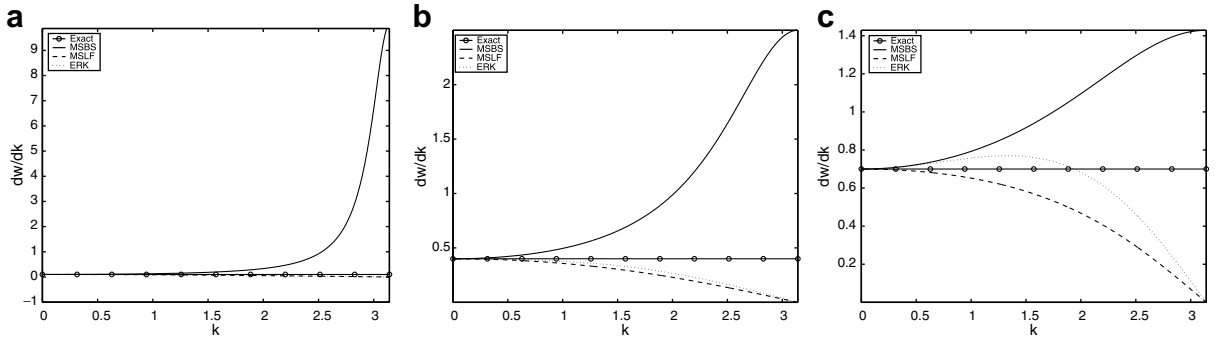

Fig. 2. Group velocities for the MSBS, MSLF and ERK schemes for (a) $\lambda = 0.1$, (b) $\lambda = 0.4$ and (c) $\lambda = 0.7$.

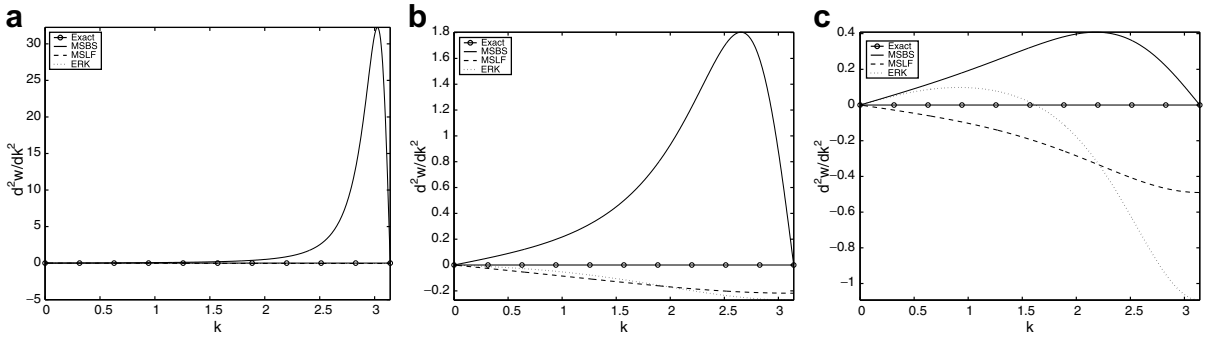

Fig. 3. Group velocity dispersion curves for the MSBS, MSLF and ERK schemes for (a) $\lambda = 0.1$, (b) $\lambda = 0.4$ and (c) $\lambda = 0.7$. Since $\bar{\omega}'' \not\equiv 0$ the discretizations introduce artificial dispersion.

dispersive properties of the schemes are distinct. The dispersion curve for the MSBS (MSLF) scheme is above (below) the analytical dispersion curve. That is,

$$\bar{\omega}_{\mathrm{BS}} > \bar{\omega}_{\mathrm{analytic}} > \bar{\omega}_{\mathrm{LF}} \quad \forall \bar{k} \in (0,\pi) \text{ and } \lambda \in (0,1). \tag{32}$$

Although the dispersion curves for MSLF and ERK appear very close for small λ, this is not always the case as the dispersion curve for ERK transitions from above to below the analytical curve at a value of the wavenumber $\bar{k}$ that depends on λ.

The dispersion curves are all monotonically increasing at rates given by their numerical group velocities (see Fig. 2)

$$\mathrm{MSBS}: \quad \bar{\omega}'(\bar{k}) = \lambda\left(\frac{1+\tan^2\bar{k}/2}{1+\lambda^2\tan^2\bar{k}/2}\right) > \lambda \quad \forall \bar{k}, \tag{33a}$$

$$\mathrm{MSLF}: \quad \bar{\omega}'(\bar{k}) = \lambda\left(\frac{1-\sin^2\bar{k}/2}{1-\lambda^2\sin^2\bar{k}/2}\right)^{1/2} < \lambda \quad \forall\, \bar{k}, \tag{33b}$$

$$\mathrm{ERK}: \quad \bar{\omega}'(\bar{k}) = \lambda\frac{\cos\bar{k}/2(1+2\lambda^2\sin^2\bar{k}/2)}{(1-2\lambda^4\sin^4\bar{k}/2-\lambda^6\sin^6\bar{k}/2)^{1/2}} \tag{33c}$$

for $0 < \bar{k} < \pi$. Fig. 2 shows the group velocities $\bar{\omega}'(\bar{k})$ for the MSBS, MSLF and ERK schemes as well as the exact group velocity (which is a constant) for $\lambda = 0.1, 0.4, 0.7$. We find that $\forall\lambda < 1$ and $\forall\bar{k} \in (0,\pi)$,

$$V_g^{\mathrm{MSBS}} > V_g^{\mathrm{analytic}} > V_g^{\mathrm{MSFL}} > 0,$$

where to simplify notation we let $\bar{\omega}'(\bar{k}) = V_g^{\mathrm{scheme}}$. As with the dispersion curves, the group velocity for ERK transitions from above to below the analytical group velocity at a value of the wavenumber $\bar{k}$ that depends on λ. Moreover, the error in $\bar{\omega}(\bar{k})$ is inversely related to λ for the MSBS and directly related to λ for the MSLF. For MSBS (MSLF), the error in the group velocity is a decreasing (increasing) function of λ.

All the numerical group velocities are positive and so this feature alone does not explain the different behavior observed in the numerical simulations of the wave and sine-Gordon equations (see Section 4.3). What can be easily correlated to the behavior of the schemes is the sign of the second derivative (see Fig. 3)

$$\mathrm{MSBS}: \quad \bar{\omega}''(\bar{k}) = \lambda(1-\lambda^2)\ \tan\bar{k}/2\left(\frac{\sec\bar{k}/2}{1+\lambda^2\tan^2\bar{k}/2}\right)^2 > 0, \tag{34a}$$

$$\mathrm{MSLF}: \quad \bar{\omega}''(\bar{k}) = -\frac{1}{2}\lambda(1-\lambda^2)\frac{\sin\bar{k}/2}{(1-\lambda^2\sin^2\bar{k}/2)^{3/2}} < 0 \tag{34b}$$

for $0 < \bar{k} < \pi$. Fig. 3 shows the group velocity dispersion curves, $\bar{\omega}''(\bar{k})$, for the MSBS, MSLF and ERK schemes for $\lambda = 0.1$, $\lambda = 0.4$ and $\lambda = 0.7$. For MSBS, $\bar{\omega}''(\bar{k}) > 0\ \forall\bar{k}$, and the group velocity curve is monotonically increasing. The higher the wavenumber $\bar{k}$ of a mode, the faster the mode travels. Further, since $\bar{\omega}'(0) = \lambda$, all

the numerical modes travel faster than the analytical ones. For MSLF, $\bar{\omega}''(\bar{k}) < 0\ \forall \bar{k}$, and the group velocity curve is monotonically decreasing. Since $\bar{\omega}'(0) = \lambda$, all the numerical modes travel slower than the analytical ones.

These results can be summarized in the following corollary:

Corollary 1. *Consider the numerical solution of the non-dispersive wave equation given by the MSBS and MSLF schemes. Then the numerical dispersion relations satisfy*

1. *The dispersion curve for the MSBS (MSLF) scheme is above (below) the analytical dispersion curve.*
2. *The sign of the analytical group velocity is preserved under the box and leapfrog schemes. Furthermore*

$$\frac{\bar{\omega}_{\mathrm{BS}}}{d\bar{k}} > \lambda > \frac{\bar{\omega}_{\mathrm{LF}}}{d\bar{k}} > 0,$$

   where λ corresponds to the analytical group velocity in the $\bar{k}$–$\bar{\omega}$ coordinate system.
3. *The error in the group velocity due to the box (leapfrog) scheme is a decreasing (increasing) function of λ.*
4. *The box (leapfrog) scheme introduces positive (negative) dispersion.*

4.3. The linearized sine-Gordon equation

The linearized sine-Gordon equation provides another example of the relevance of the numerical dispersion relation. Fig. 4(a) shows (28a) and (29), the numerical dispersion relations for (24) with ($\chi = 1$). From a cursory inspection of Fig. 4(a), the curves do not appear that different from the dispersion relation for the wave equation in Fig. 1. However, in Fig. 4(b) a magnification of the error in the dispersion relation, $\epsilon = \bar{\omega}_{\mathrm{num}} - \bar{\omega}_{\mathrm{analytic}}$, reveals that for small values of $\bar{k}$ the numerical dispersion relations for the wave and linearized sG equations differ in a small but significant aspect. For the linearized sG, the inequality relating the numerical and analytical dispersion relations is not valid for all values of $\bar{k}$, as it was for the wave Eq. (32). Instead, for small $\bar{k}$, the inequality is reversed. We obtain

$$\bar{\omega}_{\mathrm{BS}} < \bar{\omega}_{\mathrm{analytic}} < \bar{\omega}_{\mathrm{LF}}, \quad \bar{k} \in (0, \bar{k}_\lambda) \text{ and } \lambda \in (0,1), \tag{35a}$$

$$\bar{\omega}_{\mathrm{BS}} > \bar{\omega}_{\mathrm{analytic}} > \bar{\omega}_{\mathrm{LF}}, \quad \bar{k} \in (\bar{k}_\lambda, \pi) \text{ and } \lambda \in (0,1), \tag{35b}$$

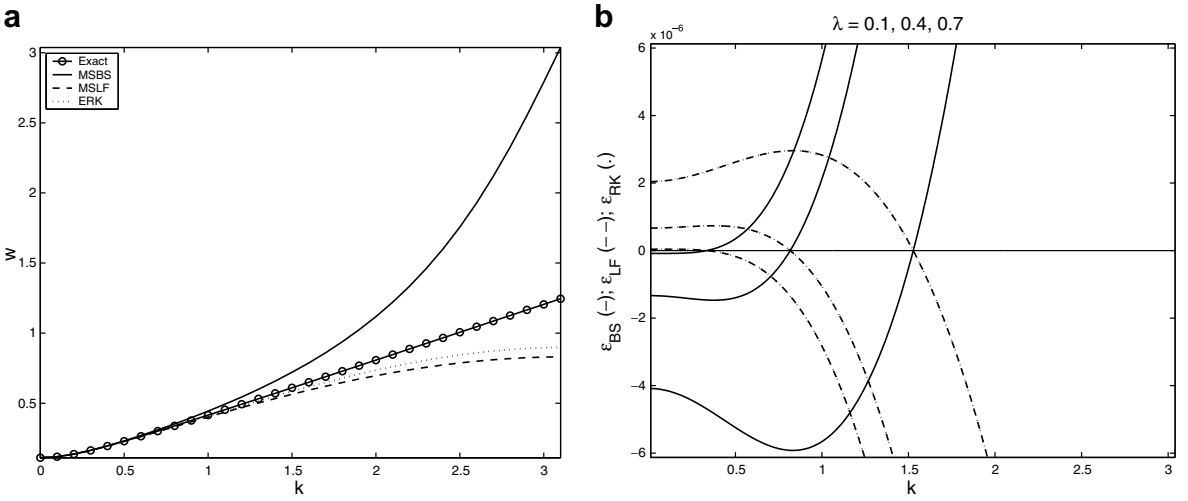

Fig. 4. Dispersion relation for the sine-Gordon equation. (a) Dispersion relation for linearized sG, $\lambda = 0.4$. (b) Dispersion relation errors ϵ_{BS}, ϵ_{LF} and ϵ_{RK}.

where $\bar{k}_\lambda$ is an increasing function of λ. A similar inequality holds when $\bar{\omega}_{\mathrm{LF}}$ is replaced by $\bar{\omega}_{\mathrm{RK}}$ in equations (35).

Inequalities (35) are significant when numerically integrating the linearized sG equation as the total energy can be characterized in terms of the group velocity $\bar{\omega}$. Following Whitham [22], we find that the exact total energy is

$$E_{\mathrm{analytic}} = 2\pi \int_0^\pi [\omega^2 \Phi_0^2(\kappa) + \Phi_1^2(\kappa)] \mathrm{d}\kappa, \tag{36}$$

where Φ_0 and Φ_1 are the Fourier coefficients for the initial conditions $u(x,0)$ and $u_t(x,0)$. Since initially the energy is concentrated in the lower modes, from Fig. 4(b), we conclude that

$$E_{\mathrm{MSBS}} < E_{\mathrm{analytic}} < E_{\mathrm{MSLF}}. \tag{37}$$

Eq. (37) also holds when E_{MSLF} is replaced by E_{ERK}. The energy inequality is a critical issue in the simulation of non-dispersive solutions of the sG equation, where their existence relies on the balance of nonlinear and dispersive effects and the preservation of energy. Once this balance is altered, changes in the energy can result in significant changes in the solutions.

5. Numerical examples

5.1. The linear wave equation

To illustrate how errors in the dispersion relation associated with MS discretization impact traveling solutions we consider the wave Eq. (24) ($\chi = 0$) with whole line B.C. for initial data characterized by a broad Fourier spectrum,

$$u(x,0) = f(x) = \exp(-3200x^2), \quad u_t(x,0) = 0, \tag{38}$$

as shown in Fig. 5(a). Fig. 5(b–d) show the numerical results obtained with MSBS, MSLF, and ERK, respectively, at $t = 0.6$ with $J = 256$, $\lambda = 0.1$ and a simulation period of $L = 2$. One would expect to obtain two wave forms of the same shape as the initial Gaussian data, with smaller amplitudes and traveling in opposite directions, i.e. $u(x,t) = \frac{1}{2}[f(x+ct) + f(x-ct)]$. Instead, we find the initial waveform rapidly disperses into a periodic wave-train. This phenomenon is explained by the error in the group velocity due to the discretizations. Since the error in the propagation speed for the MSBS scheme is positive (Fig. 2(a)), the higher wavenumber

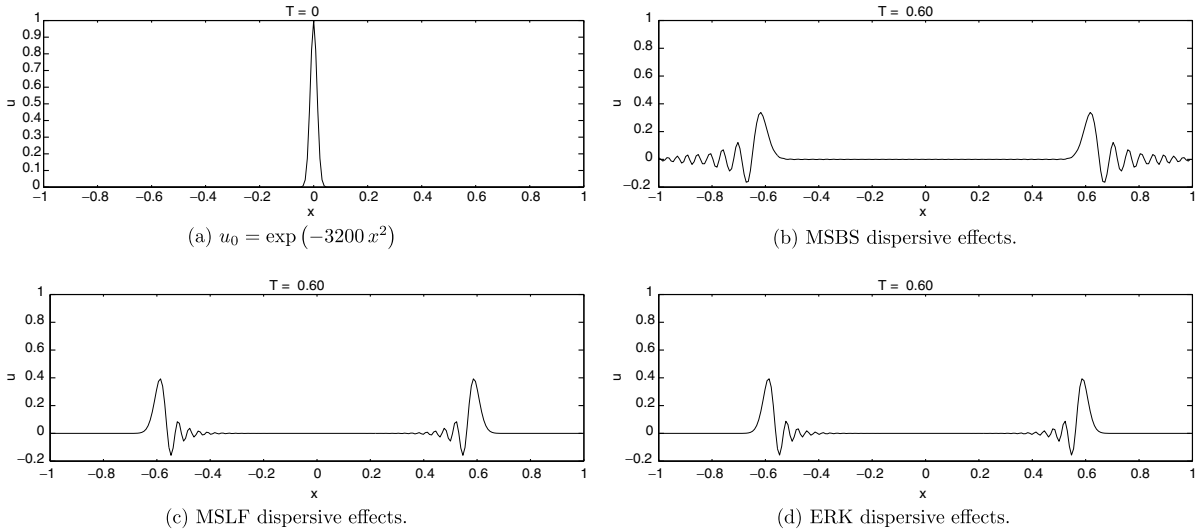

(a) $u_0 = \exp(-3200\,x^2)$ (b) MSBS dispersive effects.

(c) MSLF dispersive effects. (d) ERK dispersive effects.

Fig. 5. Dispersive error in the linear wave equation, $J = 256$, $\lambda = 0.1$.

modes travel faster than the analytical ones, while for the MSLF and ERK schemes the error is negative for the higher wavenumber modes, indicating they travel slower. In the numerical simulations the MSBS wavefront travels slower than the high-frequency oscillations as predicted by the analysis (Fig. 5(b)) whereas the opposite phenomenon is observed for MSLF and the ERK schemes (Fig. 5(c and d)). The MSBS high mode oscillations travel further than the MSLF or ERK oscillations due to a larger magnitude in the error of the group velocity.

Fig. 6 provides a comparison of the results obtained with MSLF and ERK for initial data (38) at $t = 0.2$ with $\lambda = 0.7, J = 512$ and a simulation period of $L = 2$. Although the solutions obtained with the MSLF and ERK are close for $\lambda = 0.1$, this is not the case for larger λ. The front of the ERK solution, comprised of the low wavenumber modes, travels slightly faster than that of the MSLF (or analytical) solution, while high mode oscillations develop behind the structure when using ERK. To display these features more effectively Fig. 6(a) zooms in on the peaks of the waveform while Fig. 6(b) zooms in on the base of the left traveling waveform centered at $x = -0.2$. Fig. 6(a) shows that, in contrast with the MSLF solution, the amplitude of the ERK solution is growing, and the solution breaks down shortly afterwards. The MSLF correctly resolves the amplitude of the solution, has a better resolution of the group velocity and does not yet have high-frequency oscillations. The main disadvantage of using the ERK scheme is that, unlike the multisymplectic schemes MSLF and MSBS which are stable for $\lambda \leqslant 1$ [17], the ERK is unstable and the dispersive errors are quickly overshadowed by the instability.

5.2. The sine-Gordon equation

Numerically induced dispersive effects such as high-frequency oscillations are also observed in simulations of the nonlinear sine-Gordon equation. The sine-Gordon equation admits families of non-dispersive multi-soliton solutions which can be obtained using either the inverse scattering transform or the Backlund transform [1]. For example, the 2-soliton solution

$$u(x,t) = 4\tan^{-1}[t\,\mathrm{sech}(x)], \quad -\infty < x < \infty \tag{39}$$

called the double-pole soliton, represents a special limiting case between a kink–antikink solution and a breather solution. Initial data for this family of solutions is given by

$$u(x,0) = 0, \quad u_t(x,0) = 4\gamma\,\mathrm{sech}(\gamma x), \tag{40}$$

where the breathers, the double-pole soliton, and the kink–antikinks, correspond to $0 < \gamma < 1$, $\gamma = 1$, and $\gamma > 1$, respectively. Breathers are stationary waves that are localized in space and periodic in time, while

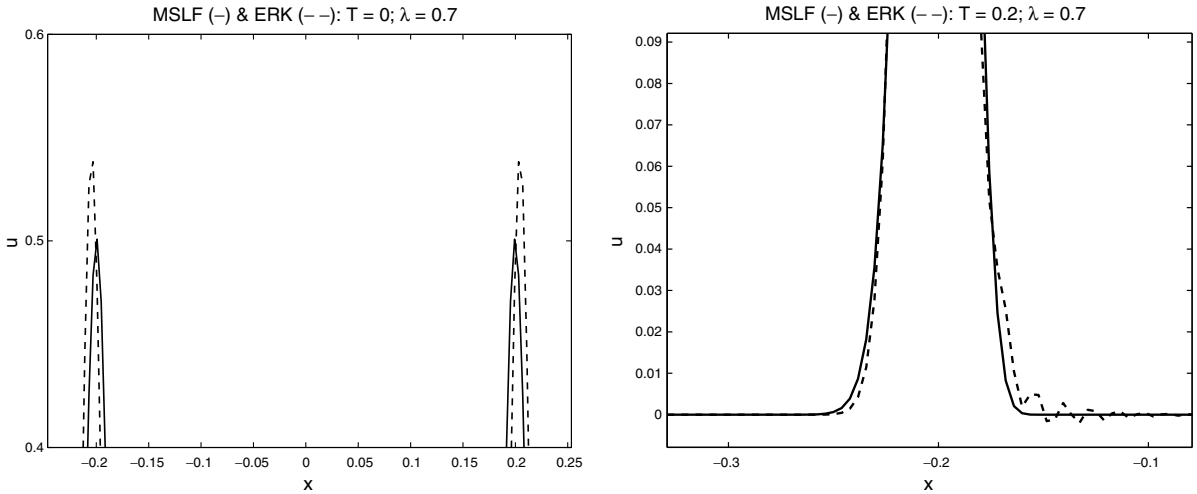

(a) Error in the front location.

(b) Development of high-frequency oscillations.

Fig. 6. Errors due to the transition point in the dispersion relation for ERK.

kink–antikinks are two-soliton waves consisting of two fronts traveling in opposite directions in space. The energy, equal to 16γ, for this family of solutions is an increasing function of γ, i.e. breathers are of lower energy than the double-pole soliton which in turn has lower energy than kink–antikink solutions.

Using initial values (40), with $\gamma = 2$ for $x \in [-20, 20]$ and periodic boundary conditions, we solve the sine-Gordon equation using the MSBS and MSLF schemes with $J = 2^n$, $n = 6, \ldots, 10$, and $\lambda = 0.1, 0.4, 0.7, 0.8,$ and 0.95. Although the kink–antikink structure is resolved by these schemes, the insets in Fig. 7(a) and (b) show small oscillatory waves developing. In the enlargements we see that the oscillations develop ahead (MSBS) or behind (MSLF) the kink–antikink front, just as in the previous linear wave equation example. These spurious effects are explained by the numerical dispersion relation associated with each MS discretization (see Fig. 4(a)).

Assuming a sufficiently small λ for a given timeframe to prevent the growth of instabilities, the dispersive effects in solitons using the ERK is qualitatively similar to MSLF in that the oscillatory waves that develop on the kink–antikink structure are behind the front as they were for the MSLF.

A more dramatic example of the impact errors in the dispersion relation have on the solution is provided by the double-pole soliton of the sine-Gordon equation. Consider the double-pole initial data

$$u(x,0) = 0, \quad u_t(x,0) = 4\mathrm{sech}(x), \tag{41}$$

with $x \in [-20, 20]$ and periodic boundary conditions. The solutions obtained using the MSBS and MSLF schemes for the sine-Gordon equation for $0 \leqslant t \leqslant 100$ are shown in Fig. 8. Although the numerical solutions converge to the double-pole soliton as the mesh is refined (here $\lambda = 0.1$), there is a notable difference in the qualitative features of the solution depending upon which numerical method was applied. Fig. 8(a) shows that a breather solution is obtained with the MSBS, while Fig. 8(b) shows a kink–antikink solution is obtained with the MSLF scheme. These distinct discrete solutions are always obtained with the respective schemes as the mesh is refined, independent of the choice of either λ, Δx or Δt. For $\lambda = 0.1$ the ERK scheme produces kink–antikink solutions similar to the MSLF solutions and are not shown since the surface plots are visually identical to those in Fig. 8(b). The ERK scheme should not be used for large λ as it is unstable and large amplitude oscillations destroy the solution on this timeframe.

Convergence to the double-pole soliton solution from different nearby solutions can be explained by analyzing the total energy, E, associated with the linearized sine-Gordon equation. Initially, in the linear regime, the double-pole soliton evolves according to the linearized sine-Gordon equation with total energy given by Eq. (36). The numerical total energies are related to the analytical energy by inequality (37). On the other hand, the energies associated with breathers, double-poles and kink–antikinks are related to each other by (see for example, [1])

$$E_{\text{breather}} < E_{\text{double-pole}} < E_{\text{kink–antikink}}.$$

From this we conclude the numerical solution obtained with the MSBS scheme will be a breather solution while the one obtained with the MSLF or ERK schemes will be a kink–antikink solution. Fig. 9(a and b) show the Hamiltonian functional discretized to fourth order accuracy. Fig. 9(a) shows the numerical energy of the

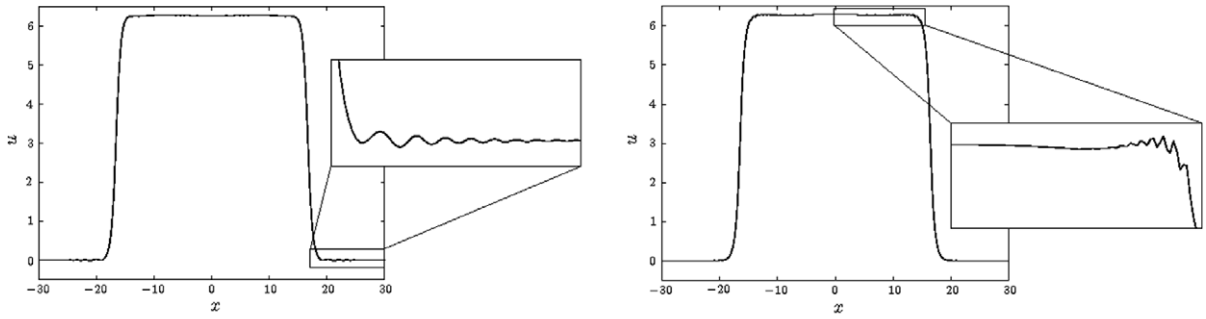

(a) MSBS dispersive effects (b) MSLF dispersive effects

Fig. 7. Dispersive effects in solitons.

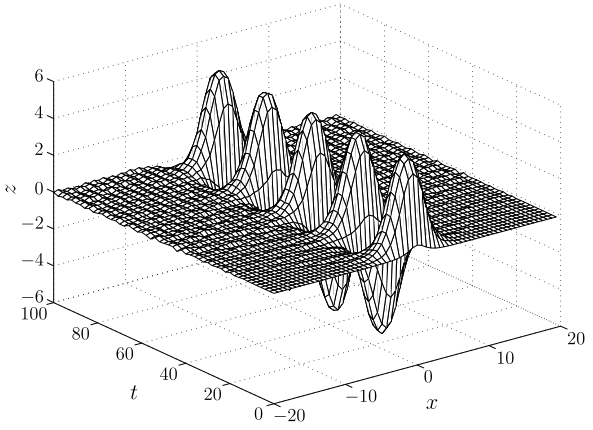

(a) MSBS, $J = 64$, $\Delta t = 64 \cdot 10^{-3}$.

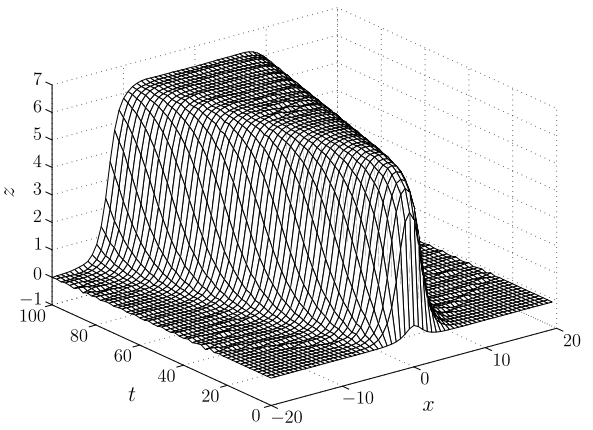

(b) MSLF, $J = 64$, $\Delta t = 64 \cdot 10^{-3}$.

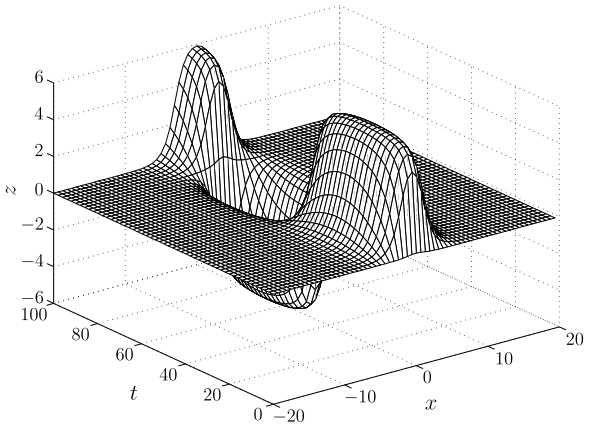

(c) MSBS, $J = 256$, $\Delta t = 16 \cdot 10^{-3}$.

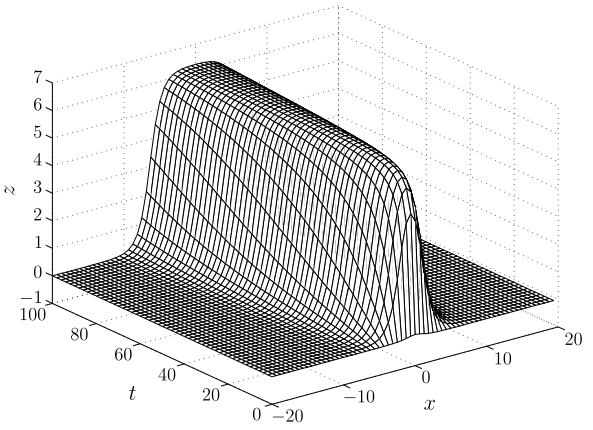

(d) MSLF, $J = 256$, $\Delta t = 16 \cdot 10^{-3}$.

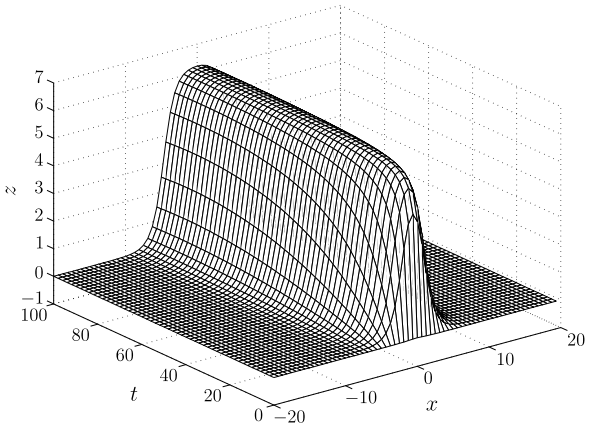

(e) MSBS, $J = 1024$, $\Delta t = 4 \cdot 10^{-3}$.

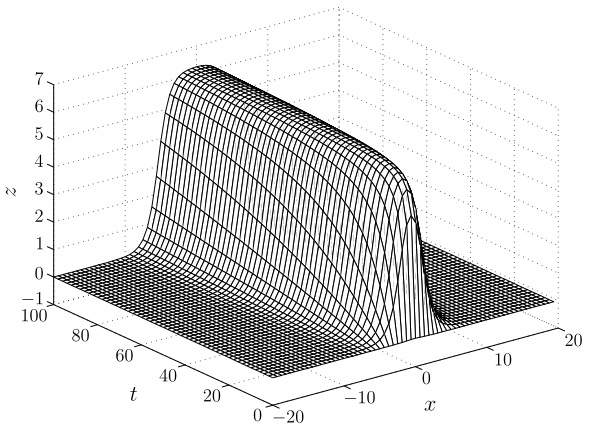

(f) MSLF, $J = 1024$, $\Delta t = 4 \cdot 10^{-3}$.

Fig. 8. Convergence of the numerical solution obtained with (a) the MSBS or (b) the MSLF scheme to the double-pole soliton solution of the sine-Gordon equation.

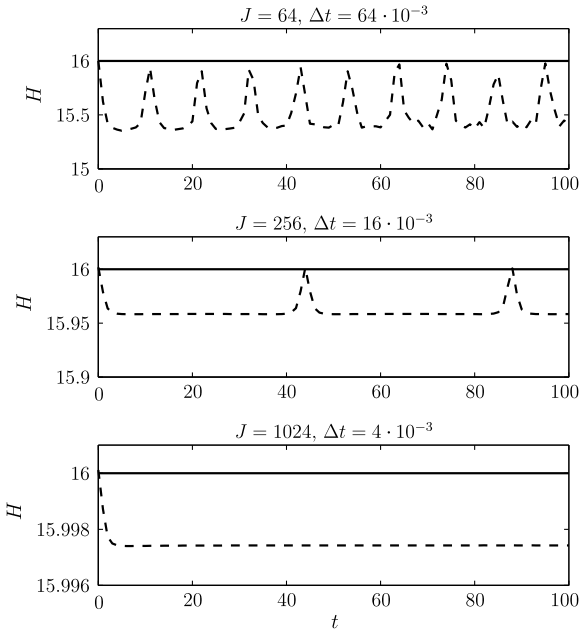

(a) Energy evolution for MSBS as the mesh is refined.

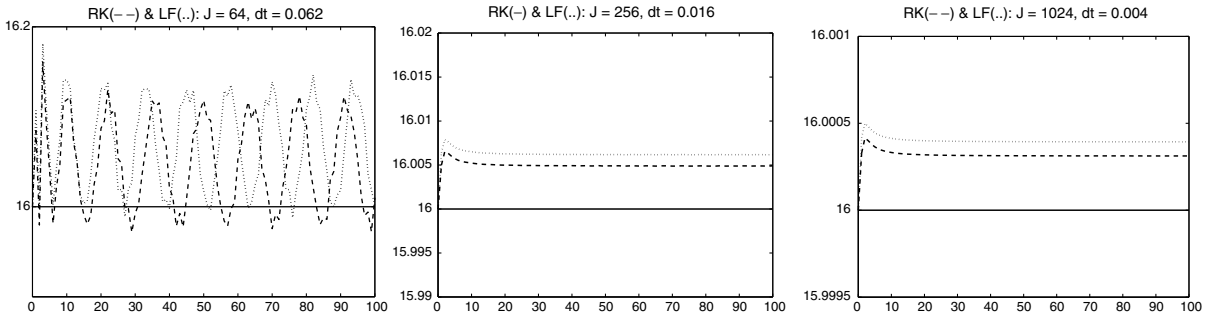

(b) Energy evolution for MSLF and ERK schemes as the mesh is refined.

Fig. 9. Convergence of the energy to that of the double-pole soliton for (a) the MSBS and (b) the MSLF and ERK schemes.

MSBS (dashed line) is less than or equal to the analytical one (solid line) for all times, while Fig. 9(b) shows the numerical energies of the MSLF and ERK schemes (dotted and dashed line, respectively) are greater than or equal to the analytical one. Again, this feature is independent of the mesh size and confirms the previous dispersion and energy analysis, that the perturbation introduced by the MS map forces the numerical solutions to lie in the region of the phase space that corresponds to a lower energy state (breather) or a higher energy state (kink–antikink) depending solely upon the discretization.

References

[1] M.J. Ablowitz, H. Segur, Solitons and the Inverse Scattering Transform, SIAM, Philadelphia, 1981.
[2] U.M. Asher, R.I. McLachlan, Multisymplectic box scheme and the Kortweg–de Vries equation, Appl. Numer. Math. 48 (2004) 255–269.
[3] U.M. Ascher, R.I. McLachlan, On symplectic and multisymplectic schemes for the KDV equation, J. Sci. Comput. 25 (2005) 83–104.
[4] T.J. Bridges, A geometric formulation of the conservation of wave action and its implications for signature and the classification of instabilities, Proc. Roy. Soc. London Ser. A 453 (1997) 1365–1395.
[5] T.J. Bridges, G. Derks, Unstable eigenvalues and the linearization about solitary waves and fronts with symmetry, R. Soc. Lond. Proc. Ser. A Math. Phys. Eng. Sci. 455 (1999) 2427–2469.

[6] T.J. Bridges, S. Reich, Multi-symplectic integrators: numerical schemes for Hamiltonian PDEs that conserve symplecticity, Phys. Lett. A 284 (2001) 184–193.
[8] T.J. Bridges, S. Reich, Numerical Methods for Hamiltonian PDEs, preprint, 2006.
[9] J. Frank, Conservation of wave action under multisymplectic discretizations, J. Phys. A 39 (2006) 5479–5493.
[10] J. Frank, B.E. Moore, S. Reich, Linear PDEs and numerical methods that preserve a multisymplectic conservation law, SIAM J. Sci. Comput. 28 (2006) 260–277.
[11] E. Hairer, Ch. Lubich, G. Wanner, Geometric Numerical Integration: Structure Preserving Algorithms for Ordinary Differential Equations, Springer-Verlag, Berlin, 2002.
[12] A.L. Islas, D.A. Karpeev, C.M. Schober, J. Comput. Phys. 173 (2001) 116–148.
[14] A.L. Islas, C.M. Schober, On the preservation of phase space structure under multisymplectic discretization, J. Comput. Phys. 197 (2004) 585–609.
[15] J.E. Marsden, G.P. Patrick, S. Shkoller, Multisymplectic geometry, variational integrators and nonlinear PDEs, Commun. Math. Phys. 199 (1999) 351–395.
[16] B.E. Moore, S. Reich, Backward error analysis for multi-symplectic integrators, Numer. Math. 95 (2003) 625–652.
[17] J.W. Thomas, Numerical Partial Differential Equations, Springer, 1995 (Press 2007).
[18] T.H. Wlodarczyk, Stability and Preservation Properties of Multisymplectic Integrators, Ph.D. Thesis, UCF, 2007.
[19] S. Reich, Multisymplectic Runge–Kutta collocation methods for Hamiltonian wave equations, J. Comput. Phys. 157 (2000) 473–499.
[20] B.N. Ryland, R.I. Mclachlan, J. Frank, On multisymplecticity of partition Runge–Kutta and splitting methods, preprint, 2006.
[21] L.N. Trefethen, Group velocities in finite difference schemes, SIAM Rev. 24 (1982) 113–136.
[22] G.B. Whitham, Linear and Nonlinear Waves, Wiley-Interscience, New York, 1974.